Biomedical Optics EXPRESS

Quantitative assessment of oral mucosa and labial minor salivary glands in patients with Sjögren's syndrome using swept source OCT

Ireneusz Grulkowski,[1,*] Jan K. Nowak,[2] Karol Karnowski,[1] Paweł Zebryk,[3] Mariusz Puszczewicz,[3] Jaroslaw Walkowiak,[2] and Maciej Wojtkowski[1]

[1]*Institute of Physics, Faculty of Physics, Astronomy and Informatics, Nicolaus Copernicus University, ul. Grudziadzka 5, 87-100 Toruń, Poland*

[2]*Department of Pediatric Gastroenterology and Metabolic Diseases, Poznań University of Medical Sciences, ul. Szpitalna 27/33, 60-572 Poznań, Poland*

[3]*Department of Rheumatology and Internal Diseases, Poznań University of Medical Sciences, ul. 28 Czerwca 1956 r. 135/147, 61-545 Poznań, Poland*

[*]*igrulkowski@fizyka.umk.pl*

Abstract: Three-dimensional imaging of the mucosa of the lower lip and labial minor salivary glands is demonstrated *in vivo* using swept source optical coherence tomography (OCT) system at 1310 nm with modified interface. Volumetric data sets of the inner surface of the lower lip covering ~230 mm^2 field are obtained from patients with Sjögren's syndrome and a control group. OCT enables high-resolution visualization of mucosal architecture using cross-sectional images as well as en-face projection images. Comprehensive morphometry of the labial minor salivary glands is performed, and statistical significance is assessed. Statistically significant differences in morphometric parameters are found when subgroups of patients with Sjögren's syndrome are analyzed.

OCIS codes: (110.4500) Optical coherence tomography; (170.3880) Medical and biological imaging; (170.4580) Optical diagnostics for medicine; (170.6930) Tissue.

References and links

1. A. Tincani, L. Andreoli, I. Cavazzana, A. Doria, M. Favero, M.-G. Fenini, F. Franceschini, A. Lojacono, G. Nascimbeni, A. Santoro, F. Semeraro, P. Toniati, and Y. Shoenfeld, "Novel aspects of Sjögren's syndrome in 2012," BMC Med. **11**(1), 93 (2013).
2. C. Baldini, R. Talarico, A. G. Tzioufas, and S. Bombardieri, "Classification criteria for Sjogren's syndrome: a critical review," J. Autoimmun. **39**(1-2), 9–14 (2012).
3. Y. Shapira, N. Agmon-Levin, and Y. Shoenfeld, "Geoepidemiology of autoimmune rheumatic diseases," Nat Rev Rheumatol **6**(8), 468–476 (2010).
4. S. A. Mathews, B. T. Kurien, and R. H. Scofield, "Oral Manifestations of Sjögren's Syndrome," J. Dent. Res. **87**(4), 308–318 (2008).
5. M. Bell, A. Askari, A. Bookman, S. Frydrych, J. Lamont, J. McComb, C. Muscoplat, and A. Slomovic, "Sjögren's syndrome: A critical review of clinical management," J. Rheumatol. **26**(9), 2051–2061 (1999).
6. M. Lee, J. A. Rutka, A. R. Slomovic, J. McComb, D. J. Bailey, and A. A. M. Bookman, "Establishing guidelines for the role of minor salivary gland biopsy in clinical practice for Sjögren's syndrome," J. Rheumatol. **25**(2), 247–253 (1998).
7. D. Guellec, D. Cornec, S. Jousse-Joulin, T. Marhadour, P. Marcorelles, J.-O. Pers, A. Saraux, and V. Devauchelle-Pensec, "Diagnostic value of labial minor salivary gland biopsy for Sjögren's syndrome: A systematic review," Autoimmun. Rev. **12**(3), 416–420 (2013).
8. S. Y. Lee, S. J. Han, S. M. Nam, S. C. Yoon, J. M. Ahn, T.-I. Kim, E. K. Kim, and K. Y. Seo, "Analysis of tear cytokines and clinical correlations in Sjögren cyndrome dry eye patients and non-Sjögren syndrome dry eye patients," Am. J. Ophthalmol. **156**(2), 247–253 (2013).
9. S. C. Shiboski, C. H. Shiboski, L. A. Criswell, A. N. Baer, S. Challacombe, H. Lanfranchi, M. Schiødt, H. Umehara, F. Vivino, Y. Zhao, Y. Dong, D. Greenspan, A. M. Heidenreich, P. Helin, B. Kirkham, K. Kitagawa, G. Larkin, M. Li, T. Lietman, J. Lindegaard, N. McNamara, K. Sack, P. Shirlaw, S. Sugai, C. Vollenweider, J. Whitcher, A. Wu, S. Zhang, W. Zhang, J. S. Greenspan, and T. E. Daniels, "American College of Rheumatology

#199754 - $15.00 USD Received 23 Oct 2013; revised 26 Nov 2013; accepted 26 Nov 2013; published 16 Dec 2013

classification criteria for Sjögren's syndrome: A data-driven, expert consensus approach in the Sjögren's International Collaborative Clinical Alliance Cohort," Arth. Care Res. **64**(4), 475–487 (2012).
10. C. J. Burke, R. H. Thomas, and D. Howlett, "Imaging the major salivary glands," Br. J. Oral Maxillofac. Surg. **49**(4), 261–269 (2011).
11. W. W. I. Kalk, A. Vissink, F. K. L. Spijkervet, H. Bootsma, C. G. M. Kallenberg, and J. L. N. Roodenburg, "Parotid sialography for diagnosing Sjögren syndrome," Oral Surg. Oral Med. Oral Pathol. Oral Radiol. Endod. **94**(1), 131–137 (2002).
12. L. S. de Clerck, R. Corthouts, L. Francx, C. Brussaard, A. de Schepper, H. A. Vercruysse, and W. J. Stevens, "Ultrasonography and computer tomography of the salivary glands in the evaluation of Sjögren's syndrome. comparison with parotid sialography," J. Rheumatol. **15**(12), 1777–1781 (1988).
13. I. Umehara, I. Yamada, Y. Murata, Y. Takahashi, N. Okada, and H. Shibuya, "Quantitative evaluation of salivary gland scintigraphy in Sjörgen's syndrome," J. Nucl. Med. **40**(1), 64–69 (1999).
14. H. Tonami, K. Higashi, M. Matoba, H. Yokota, I. Yamamoto, and S. Sugai, "A comparative study between MR sialography and salivary gland scintigraphy in the diagnosis of Sjögren syndrome," J. Comput. Assist. Tomogr. **25**(2), 262–268 (2001).
15. P. Zengel, F. Schrötzlmair, C. Reichel, P. Paprottka, and D. A. Clevert, "Sonography: The Leading Diagnostic Tool for Diseases of the Salivary Glands," Semin. Ultrasound CT MR **34**(3), 196–203 (2013).
16. M. Sumi, T. Yamada, Y. Takagi, and T. Nakamura, "MR imaging of labial glands," AJNR Am. J. Neuroradiol. **28**(8), 1552–1556 (2007).
17. A. Uchugonova and K. König, "Two-photon autofluorescence and second-harmonic imaging of adult stem cells," J. Biomed. Opt. **13**(5), 054068 (2008).
18. D. Beroukas, J. Hiscock, R. Jonsson, S. A. Waterman, and T. P. Gordon, "Subcellular distribution of aquaporin 5 in salivary glands in primary Sjögren's syndrome," Lancet **358**(9296), 1875–1876 (2001).
19. D. Huang, E. A. Swanson, C. P. Lin, J. S. Schuman, W. G. Stinson, W. Chang, M. R. Hee, T. Flotte, K. Gregory, C. A. Puliafito, and J. G. Fujimoto, "Optical coherence tomography," Science **254**(5035), 1178–1181 (1991).
20. T. H. Ko, D. C. Adler, J. G. Fujimoto, D. Mamedov, V. Prokhorov, V. Shidlovski, and S. Yakubovich, "Ultrahigh resolution optical coherence tomography imaging with a broadband superluminescent diode light source," Opt. Express **12**(10), 2112–2119 (2004).
21. R. A. Leitgeb, W. Drexler, A. Unterhuber, B. Hermann, T. Bajraszewski, T. Le, A. Stingl, and A. F. Fercher, "Ultrahigh resolution Fourier domain optical coherence tomography," Opt. Express **12**(10), 2156–2165 (2004).
22. W. Wieser, B. R. Biedermann, T. Klein, C. M. Eigenwillig, and R. Huber, "Multi-Megahertz OCT: High quality 3D imaging at 20 million A-scans and 4.5 GVoxels per second," Opt. Express **18**(14), 14685–14704 (2010).
23. M. Wojtkowski, "High-speed optical coherence tomography: basics and applications," Appl. Opt. **49**(16), D30–D61 (2010).
24. M. A. Choma, M. V. Sarunic, C. H. Yang, and J. A. Izatt, "Sensitivity advantage of swept source and Fourier domain optical coherence tomography," Opt. Express **11**(18), 2183–2189 (2003).
25. J. F. de Boer, B. Cense, B. H. Park, M. C. Pierce, G. J. Tearney, and B. E. Bouma, "Improved signal-to-noise ratio in spectral-domain compared with time-domain optical coherence tomography," Opt. Lett. **28**(21), 2067–2069 (2003).
26. R. Leitgeb, C. K. Hitzenberger, and A. F. Fercher, "Performance of fourier domain vs. time domain optical coherence tomography," Opt. Express **11**(8), 889–894 (2003).
27. S. R. Chinn, E. A. Swanson, and J. G. Fujimoto, "Optical coherence tomography using a frequency-tunable optical source," Opt. Lett. **22**(5), 340–342 (1997).
28. R. Huber, M. Wojtkowski, and J. G. Fujimoto, "Fourier Domain Mode Locking (FDML): A new laser operating regime and applications for optical coherence tomography," Opt. Express **14**(8), 3225–3237 (2006).
29. G. J. Tearney, M. E. Brezinski, B. E. Bouma, S. A. Boppart, C. Pitris, J. F. Southern, and J. G. Fujimoto, "In vivo endoscopic optical biopsy with optical coherence tomography," Science **276**(5321), 2037–2039 (1997).
30. S. A. Boppart, B. E. Bouma, C. Pitris, G. J. Tearney, J. G. Fujimoto, and M. E. Brezinski, "Forward-imaging instruments for optical coherence tomography," Opt. Lett. **22**(21), 1618–1620 (1997).
31. F. Feldchtein, G. Gelikonov, V. Gelikonov, R. Kuranov, A. Sergeev, N. Gladkova, A. Shakhov, N. Shakhova, L. Snopova, A. Terent'eva, E. Zagainova, Y. Chumakov, and I. Kuznetzova, "Endoscopic applications of optical coherence tomography," Opt. Express **3**(6), 257–270 (1998).
32. A. Sergeev, V. Gelikonov, G. Gelikonov, F. Feldchtein, R. Kuranov, N. Gladkova, N. Shakhova, L. Snopova, A. Shakhov, I. Kuznetzova, A. Denisenko, V. Pochinko, Y. Chumakov, and O. Streltzova, "In vivo endoscopic OCT imaging of precancer and cancer states of human mucosa," Opt. Express **1**(13), 432–440 (1997).
33. S. A. Boppart, A. Goodman, J. Libus, C. Pitris, C. A. Jesser, M. E. Brezinski, and J. G. Fujimoto, "High resolution imaging of endometriosis and ovarian carcinoma with optical coherence tomography: feasibility for laparoscopic-based imaging," Br. J. Obstet. Gynaecol. **106**(10), 1071–1077 (1999).
34. N. Hanna, D. Saltzman, D. Mukai, Z. Chen, S. Sasse, J. Milliken, S. Guo, W. Jung, H. Colt, and M. Brenner, "Two-dimensional and 3-dimensional optical coherence tomographic imaging of the airway, lung, and pleura," J. Thorac. Cardiovasc. Surg. **129**(3), 615–622 (2005).
35. D. C. Adler, C. Zhou, T.-H. Tsai, J. Schmitt, Q. Huang, H. Mashimo, and J. G. Fujimoto, "Three-dimensional endomicroscopy of the human colon using optical coherence tomography," Opt. Express **17**(2), 784–796 (2009).
36. E. Sattler, R. Kästle, and J. Welzel, "Optical coherence tomography in dermatology," J. Biomed. Opt. **18**(6), 061224 (2013).

#199754 - $15.00 USD Received 23 Oct 2013; revised 26 Nov 2013; accepted 26 Nov 2013; published 16 Dec 2013

37. F. I. Feldchtein, V. Gelikonov, R. Iksanov, G. Gelikonov, R. V. Kuranov, A. M. Sergeev, N. D. Gladkova, M. N. Ourutina, D. Reitze, and J. Warren, "In vivo OCT imaging of hard and soft tissue of the oral cavity," Opt. Express **3**(6), 239–250 (1998).
38. J. M. Ridgway, W. B. Armstrong, S. Guo, U. Mahmood, J. Su, R. P. Jackson, T. Shibuya, R. L. Crumley, M. Gu, Z. Chen, and B. J. F. Wong, "In vivo optical coherence tomography of the human oral cavity and oropharynx," Arch. Otolaryngol. Head Neck Surg. **132**(10), 1074–1081 (2006).
39. M. T. Tsai, H. C. Lee, C. K. Lee, C. H. Yu, H. M. Chen, C. P. Chiang, C. C. Chang, Y. M. Wang, and C. C. Yang, "Effective indicators for diagnosis of oral cancer using optical coherence tomography," Opt. Express **16**(20), 15847–15862 (2008).
40. C.-K. Lee, M.-T. Tsai, H.-C. Lee, H.-M. Chen, C.-P. Chiang, Y.-M. Wang, and C. C. Yang, "Diagnosis of oral submucous fibrosis with optical coherence tomography," J. Biomed. Opt. **14**(5), 054008 (2009).
41. N. Ozawa, Y. Sumi, K. Shimozato, C. Chong, and T. Kurabayashi, "In vivo imaging of human labial glands using advanced optical coherence tomography," Oral Surg. Oral Med. Oral Pathol. Oral Radiol. Endod. **108**(3), 425–429 (2009).
42. L. L. Otis, D. Q. Piao, C. W. Gibson, and Q. Zhu, "Quantifying labial blood flow using optical Doppler tomography," Oral Surg. Oral Med. Oral Pathol. Oral Radiol. Endod. **98**(2), 189–194 (2004).
43. C. Vitali, S. Bombardieri, R. Jonsson, H. M. Moutsopoulos, E. L. Alexander, S. E. Carsons, T. E. Daniels, P. C. Fox, R. I. Fox, S. S. Kassan, S. R. Pillemer, N. Talal, and M. H. Weisman; European Study Group on Classification Criteria for Sjögren's Syndrome, "Classification criteria for Sjögren's syndrome: a revised version of the European criteria proposed by the American-European Consensus Group," Ann. Rheum. Dis. **61**(6), 554–558 (2002).
44. A. M. Lindvall and R. Jonsson, "The salivary gland component of Sjögren's syndrome: An evaluation of diagnostic methods," Oral Surg. Oral Med. Oral Pathol. **62**(1), 32–42 (1986).
45. C. Baeteman, L. Guyot, J. Bouvenot, C. Chossegros, F. Cheynet, C. Loudot, J. Serratrice, and S. Attarian, "Should minor salivary gland biopsy still be performed?" Rev. Stomatol. Chir. Maxillofac. **109**(3), 143–147 (2008).
46. M. Lida Santiago, M. R. Seisdedos, R. N. García Salinas, A. Secco, L. Marino Claverie, L. Techera, L. Takashima, P. Aicardi, M. A. Sandi Rosales, E. Knobel, S. J. Magri, and A. C. Catalán Pellet, "Frequency of Complications and Usefulness of the Minor Salivary Gland Biopsy," Reumatol. Clín. **8**, 255–258 (2012).
47. ANSI, *American National Standard for Safe Use of Lasers ANSI Z136.1–2007* (Laser Institute of America, Orlando, 2007), pp. 1–249.
48. J. Schindelin, I. Arganda-Carreras, E. Frise, V. Kaynig, M. Longair, T. Pietzsch, S. Preibisch, C. Rueden, S. Saalfeld, B. Schmid, J.-Y. Tinevez, D. J. White, V. Hartenstein, K. Eliceiri, P. Tomancak, and A. Cardona, "Fiji: an open-source platform for biological-image analysis," Nat. Methods **9**(7), 676–682 (2012).
49. T. Inamura, C. Ino, M. Katoh, A. Kishimoto, H. Kumazawa, A. Matsumoto, and T. Yamashita, "A Simple Method to Estimate the Secretion of Saliva From Minor Salivary Glands Using Iodine-Starch Reaction," Laryngoscope **111**(2), 272–277 (2001).
50. J. Pijpe, J. M. Meijer, H. Bootsma, J. E. van der Wal, F. K. L. Spijkervet, C. G. M. Kallenberg, A. Vissink, and S. Ihrler, "Clinical and histologic evidence of salivary gland restoration supports the efficacy of rituximab treatment in Sjögren's syndrome," Arthritis Rheum. **60**(11), 3251–3256 (2009).
51. R. Bamba, N. J. Sweiss, A. J. Langerman, J. B. Taxy, and E. A. Blair, "The minor salivary gland biopsy as a diagnostic tool for Sjogren syndrome," Laryngoscope **119**(10), 1922–1926 (2009).
52. N. Iwata, T. Miyamae, M. Kikuchi, T. Kishi, R. Hara, U. Kaneko, T. Shinoki, T. Imagawa, Y. Inayama, and S. Yokota, "Clinical and histological experience of labial lip biopsy in juvenile Sjögren syndrome [in Japanese]," Nihon Rinsho Meneki Gakkai Kaishi **32**(3), 195–200 (2009).
53. P. Z. Wang, Q. Lu, S. L. Chen, and Y. H. Jiang, "[The pathological changes of lip biopsies and dental caries on Sjogren's syndrome]," Shanghai Kou Qiang Yi Xue **2**(2), 77–79 (1993).
54. A. M. Pedersen, A. Bardow, and B. Nauntofte, "Salivary changes and dental caries as potential oral markers of autoimmune salivary gland dysfunction in primary Sjogren's syndrome," BMC Clin. Pathol. **5**(1), 4 (2005).
55. A. Tandon, N. N. Singh, and G. Sreedhar, "Minor salivary glands and dental caries: Approach towards a new horizon," J. Nat. Sci. Biol. Med. **4**(2), 364–368 (2013).
56. M. García-Carrasco, A. Sisó, M. Ramos-Casals, J. Rosas, G. de la Red, V. Gil, S. Lasterra, R. Cervera, J. Font, and M. Ingelmo, "Raynaud's phenomenon in primary Sjögren's syndrome. Prevalence and clinical characteristics in a series of 320 patients," J. Rheumatol. **29**(4), 726–730 (2002).
57. Cda. M. Brasil, C. M. Ribeiro, D. D. Fonseca, L. A. Gueiros, and J. C. Leao, "Chloroquine-induced hyperpigmentation of the hard palate," Gen. Dent. **60**(2), e74–e78 (2012).
58. L. J. Dawson, V. L. Caulfield, J. B. Stanbury, A. E. Field, S. E. Christmas, and P. M. Smith, "Hydroxychloroquine therapy in patients with primary Sjögren's syndrome may improve salivary gland hypofunction by inhibition of glandular cholinesterase," Rheumatology (Oxford) **44**(4), 449–455 (2005).

1. Introduction

Sjögren's syndrome is an autoimmune disorder of the connective tissue leading to the reduction of secretory functions of salivary and lacrimal glands [1, 2]. The disease affects nearly 1.7 million people in the European Union and around 1 million people in the United

#199754 - $15.00 USD Received 23 Oct 2013; revised 26 Nov 2013; accepted 26 Nov 2013; published 16 Dec 2013

States (~90% of them are middle-aged women) [3]. The disease has two main forms: primary Sjögren's syndrome in patients with no other connective tissue disorder or secondary Sjögren's syndrome where it is associated with rheumatoid arthritis, systemic lupus erythematosus or scleroderma. Its clinical hallmark is the dryness of the oral mucosa and the ocular conjunctiva, which cause swallowing problems and compensatory increased liquid intake [4]. However, the disease has also systemic manifestations like general fatigue, inflammatory involvement of joints, kidneys, lungs, heart, liver, gastrointestinal tract, as well as Raynaud's phenomenon (fingers and toes becoming pale, then dark blue and finally bright red due to reduced blood supply and its restoration) [5]. This complex symptomatology leads to the difficulties in Sjögren's syndrome diagnostics, which may require a number of tests including eye examination (e.g. ocular staining score using lissamine green and fluorescein or Schirmer's test), lip biopsy for assessment of the salivary gland tissue, blood tests for autoantibodies, and saliva production test [4, 6–9].

Evaluation of the salivary glands' inflammation is performed with numerous imaging techniques [10]. Sialography uses x-rays and contrast agent to visualize the glands and ducts [11]. Contrast agents administered when computed tomography is performed pose a risk for patients with kidney failure [12]. Additionally, scintigraphic imaging with radionuclide can easily demonstrate the uptake and excretion functions of the glands [13, 14]. Other salivary gland imaging methods include ultrasound and magnetic resonance imaging [15, 16]. However, most of those methods are relatively invasive and are useful in visualization of only major salivary glands. Detailed morphology of salivary glands can be revealed also with optical techniques like histology, confocal microscopy or two-photon microscopy with the support of different staining methods [7, 17, 18]. Although they provide high-resolution images, an in vivo imaging is not feasible.

Optical coherence tomography (OCT) is an optical modality that enables noninvasive imaging of the internal structure of tissues with micrometer resolution [19]. Recent developments in broadband light sources and efficient detectors enabled improvement of the imaging speed and resolution, allowing for rapid *in vivo* acquisition of volumetric data [20–22]. OCT images can also achieve axial resolutions of the order of few microns and provide access to both qualitative and quantitative information on the morphology of the tissue [23]. Implementation of Fourier detection in OCT considerably increased its ability to detect very low signals coming from the imaged objects [24–26]. OCT with wavelength-tunable lasers, known as swept source OCT (SS-OCT), offers superior performance over other detection approaches because of the lower signal drop with depth, better photon detection efficiency and possibility to use dual balance detection scheme [27, 28]. The advantage of OCT over other optical imaging methods such as confocal microscopy stems from the fact that OCT uses coherence gating, thus enabling acquisition of three-dimensional (3-D) data in a simple scanning session. On the other hand, a stack of images acquired from multiple depths must be used to perform 3-D morphology reconstruction in confocal microscopy. Consequently, scanning the tissue multiple times is required.

Currently, OCT is widely utilized in ophthalmology, where it became standard imaging technique used in diagnosis of several disorders of the retina and the anterior segment of the eye [23]. That initial application of OCT was supported by the fact that the eye is composed of transparent structures so that it is relatively easy to deliver the light as well as to detect backscattered / backreflected photons. However, OCT was also used as a visualization tool of other, less transparent tissues thanks to the integration of OCT with standard instruments like catheters, endoscopes, laparoscopes, laryngoscopes and colposcopes [29–31]. Although majority of those OCT instruments operate at 1.3 μm wavelengths to enable deeper light penetration, most applications involve imaging of subsurface tissue morphology of different organs in human body. In clinical research, special attention has been paid to mucous membranes in various parts of the body since many pathological conditions appear as structural and functional abnormalities in the mucosa. Glandular structures were visualized in

#199754 - $15.00 USD Received 23 Oct 2013; revised 26 Nov 2013; accepted 26 Nov 2013; published 16 Dec 2013

the skin as well as in the mucosa of e.g. the esophagus, colon, larynx, buccal pouch, trachea, cervix and bladder [29, 32–36].

Initial studies showed that OCT can be helpful in high-resolution imaging of the soft tissues in the oral cavity [37]. OCT imaging was also used to characterize the oral mucosa microstructures in pre-cancerous abnormalities as well as in oral cancers [38–40]. Furthermore, SS-OCT with hand-held probe was demonstrated for labial gland imaging, and blood flow in human lips was also visualized with Doppler OCT [41, 42]. However, no quantitative analysis of human lips glandular structures based on OCT data has been performed yet either for the healthy subjects or diseased conditions.

The diversity of clinical presentations of Sjögren's syndrome has led to development of sets of criteria for diagnosis of the disease. In contrast to American-European Consensus Criteria on which this study is based [43], recently proposed criteria focus more on labial minor salivary gland (LMSG) biopsy by listing it as one of three objective features of Sjögren's syndrome [9]. This change highlights the proven diagnostic value of LMSG investigation. Although other modalities for LMSG and major salivary gland analysis exist [44], so far the specificity of LMSG biopsy remained unmatched [7, 45]. However, the biopsy is an invasive procedure that leads to acute and medium term complications in about 10% of patients [46]. Therefore, a new non-invasive technique of LMSG examination that would bring benefits comparable to that of biopsy is needed.

The aim of this study was to develop a SS-OCT instrument for imaging the mucosa of the lower lip and the labial minor salivary glands, along with elaboration of the imaging approach easily applicable in a clinical setting. Another goal of our study was to introduce quantitative descriptors of the morphology of LMSGs and to perform comprehensive morphometry of LMSGs in Sjögren's syndrome patients and in subjects from a control group.

2. Methods

2.1 Swept Source OCT instrument for imaging oral mucosa and labial minor salivary glands

A schematic diagram of the SS-OCT system for imaging the mucosa of the lower lip and LMSGs is demonstrated in Fig. 1. The instrument operates at central wavelength of 1310 nm, and the light is provided by a wavelength-tunable light source (Axsun Technologies Inc., Billerica, MA, USA). The sweep rate of 50 kHz determines the imaging speed of the instrument. The laser output was divided between an OCT interferometer and a sweep calibration common-path interferometer. The OCT interferometer had configuration with the circulators in both arms to minimize losses. The power incident on the tissue surface was 6.2 mW, which was consistent with American National Standard Institute standards even for eye exposure [47]. The light was focused at the tissue using a scan lens (LSM03; Thorlabs Inc., Newton, NJ, USA), and telecentric scanning was utilized. Optical signal in the OCT interferometer was detected by a dual-balance photodiode (PDB 110C, 100 MHz; Thorlabs Inc., Newton, NJ, USA). Both OCT interferometric signal and calibration signal were acquired using dual channel A/D converter with selected internal clocking rate of 100 MS/s (Gage Compuscope 14200, 14 bits; GaGe Applied Technologies Inc., Lockport, IL, USA).

The imaging depth range of the instrument was 4.6 mm in air (corresponding to 3.4 mm in tissue). The wavelength tuning range of the light source provided axial resolution of 9 μm in air (corresponding to 6.7 μm in tissue). The transverse resolution (beam spot size) of 20 μm was determined using a beam profiler (WinCamD-UCD15-1310, DataRay Inc.). The sensitivity of the system measured with well-defined attenuator in the sample arm was 109 dB, and 6 dB signal drop was observed at 3.8 mm depth in the air.

#199754 - $15.00 USD Received 23 Oct 2013; revised 26 Nov 2013; accepted 26 Nov 2013; published 16 Dec 2013

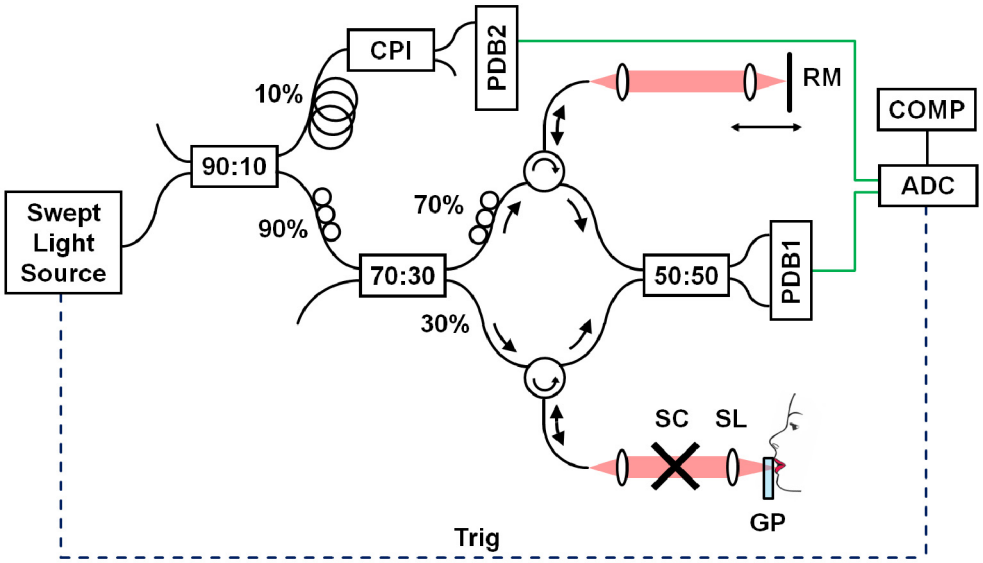

Fig. 1. Experimental SS-OCT set-up at 1310 nm. Schematic of the instrument. CPI – common path interferometer, PDB – dual-balance photodetector, RM – reference mirror, SC – galvanometric scanners, SL – scan lens, GP – glass plate, ADC – analog-to-digital converter (acquisition card), COMP – computer.

The interface of the instrument was modified to provide an easy access of the light beam to the mucosa of the lower lip. A sterile glass plate was inserted in the sample arm (Fig. 1) to enable proper exposition of the mucosa of the lower lip. The glass plate was 6 mm thick, which made it possible to avoid superposition of glass surface reflection artifacts on the signal from the tissue in OCT cross-sectional images. The glass plate was also slightly tilted during data acquisition in order to avoid strong specular reflections from the surfaces. OCT image quality was not affected by slightly unbalanced dispersion between sample and reference arms since imaging was performed at 1310 nm wavelength range, which exhibits minimum dispersion. Moreover, the distance between scan lens and glass plate was fixed and was chosen before all imaging sessions (~1 mm behind posterior surface of the glass plate) to provide optimal image quality. Therefore, the position of beam focus versus tissue surface could be fully controlled during data acquisition making quantitative measurements more objective. The application of the glass plate was also advantageous in clinical practice due to fact that the tissue touching the glass was immobilized and motion-free data sets could be easily acquired. Touching the glass with the lips was tolerated well by the patients and it significantly shortened each imaging session. Finally, OCT image post-processing did not require sophisticated segmentation tools to flatten the tissue surface in cross-sectional images.

2.2 Study group

The project was approved by the Bioethics Committees at the Nicolaus Copernicus University in Toruń (decision no KB188/213) and at the Poznań University of Medical Sciences (decision no 415/13). The study adhered to the tenets of the Declaration of Helsinki. The nature of the study was explained to all participants in detail and written consent was obtained prior to the study.

Twenty-two volunteers, all of them female, were enrolled in the study, including 11 Sjögren's syndrome patients and 11 persons in similar age and good general health. No statistically significant differences were found in group characteristics (Table 1).

#199754 - $15.00 USD Received 23 Oct 2013; revised 26 Nov 2013; accepted 26 Nov 2013; published 16 Dec 2013

Table 1. Group characteristics

Characteristics	Sjögren's syndrome	Control group
Number of persons	11	11
Age (years)	59.3 ± 11.1	54.1 ± 6.1
Body mass (kg)	66.4 ± 13.2	67.2 ± 9.8
Body height (cm)	160.1 ± 7.7	160.6 ± 6.0
Persons with allergies	3	4
Last meal (hours before OCT)	4.3 ± 3.8	4.6 ± 3.9

*Data for age, body mass, body height and time since last meal are presented as mean ± standard deviation.

A clinical questionnaire was used to gather the data necessary for the study. It consisted of two parts: the first was common for Sjögren's syndrome patients and healthy subjects and the second referred to Sjögren's syndrome patients only. The common part included questions pertaining to age, body weight and height, smoking, allergies, viral hepatitis history, hepatic disease, comorbidities, drugs taken, and time passed since last meal. A physician interviewed Sjögren's syndrome patients, and analyzed the medical documentation they provided, noting the age at diagnosis and the patient status in regard to: dryness of the oral mucosa (xerostomia), dryness of the ocular conjunctiva (keratoconjunctivitis sicca), salivary gland enlargement, autoimmune comorbidities, xerostomia-related dental disease, uveitis, joint pains (arthralgias), muscular pains (myalgias), chronic fatigue, vessel inflammation (vasculitis), Raynaud's phenomenon, interstitial lung disease, kidney disease, neuropathies, history of endocarditis and head and neck radiotherapy.

Sjögren's syndrome was diagnosed on the basis of clinical and laboratory investigations, according to a revised version of the European classification criteria for Sjögren's syndrome proposed by the American-European Consensus Group [43]. Average duration of disease was 6.2 years. All Sjögren's syndrome patients had xerostomia. Nine of them (81.8%) presented with keratoconjunctivitis sicca, 9 (81.8%) with arthralgias, 8 (72.7%) with myalgias, 7 (63.6%) with chronic fatigue, 6 (54.6%) with overlapping autoimmune comorbidities (2 – systemic lupus erythomatus, 2 – Hashimoto's thyroiditis, 1 – autoimmune hepatitis, 1 – mixed connective tissue disease, 1 – rheumatoid arthritis), 5 (45.5%) with Raynaud's phenomenon, 5 (45.5%) with xerostomia-related dental disease, 4 (36.4%) with salivary gland enlargement, and 3 (27.3%) with neuropathies. Among Sjögren's syndrome patients 7 (63.6%) took oral steroids, 4 (36.4%) chloroquine and 2 (18.2%) levothyroxine. Other drugs employed in study participants included non-steroidal anti-inflammatory drugs, angiotensin-converting enzyme inhibitors, diuretics, proton pump inhibitors, acetylsalicylic acid, atorvastatin, cetirizine, clopidogrel, fexofenadine, fluticasone, propafenone, sumatriptan and zolendronic acid. In the control group one person had asthma, one had hypertension and low-grade heart failure and one had migraines. Three Sjögren's syndrome patients and one healthy subject smoked cigarettes.

In both groups the level of anxiety immediately before OCT scanning was self-assessed by study participants using a 5-item Likert scale (1 = very anxious; 5 = not anxious at all). After OCT scanning the level of comfort during the examination was described by the participants using a 5-item Likert scale (1 = very bad; 5 = very good).

2.3 Data acquisition and processing. Statistical analysis

Each participant was instructed before starting data acquisition in order to get acquainted with the technique of touching the glass with the lips. Individual sterile glass plates were prepared for each scanned person. The procedure involved exposing the inner surface of the lower lip and to press it gently against a sterile glass plate. We obtained three wide-field volumetric SS-OCT data sets consisting of 400 × 400 A-scans and covering 17.3 × 17.3 mm^2 area. The measurement time to acquire a single volumetric data set was 3.2 seconds. The scanning area was ~2 × undersampled but the scan protocol provided both maximum field of view available

#199754 - $15.00 USD Received 23 Oct 2013; revised 26 Nov 2013; accepted 26 Nov 2013; published 16 Dec 2013

by the scanning lens and the examination time comfortable for the patients. Large scan area made it also possible to image as many salivary glands as possible and to be insensitive on the location of a lip scanning area. Thus, it gave better insight into gland morphology compared with standard salivary gland biopsy, in which conclusions are drawn only from the analysis of a single gland. Sampling the tissue does not need to be dense since to our best knowledge there are no characteristics of diseased LMSGs in Sjögren's syndrome patients that would be available by OCT.

The participant removed their head from the chinrest between imaging sessions. After processing the data, each volume was averaged using 3 × 3 pxl lateral kernel to enhance the signal and preserve high axial resolution of the cross-sectional images. In the next stage, tissue image flattening procedure with respect to the glass surface was performed, which also enabled generation of a stack of projection images (C-scans) used in further analysis.

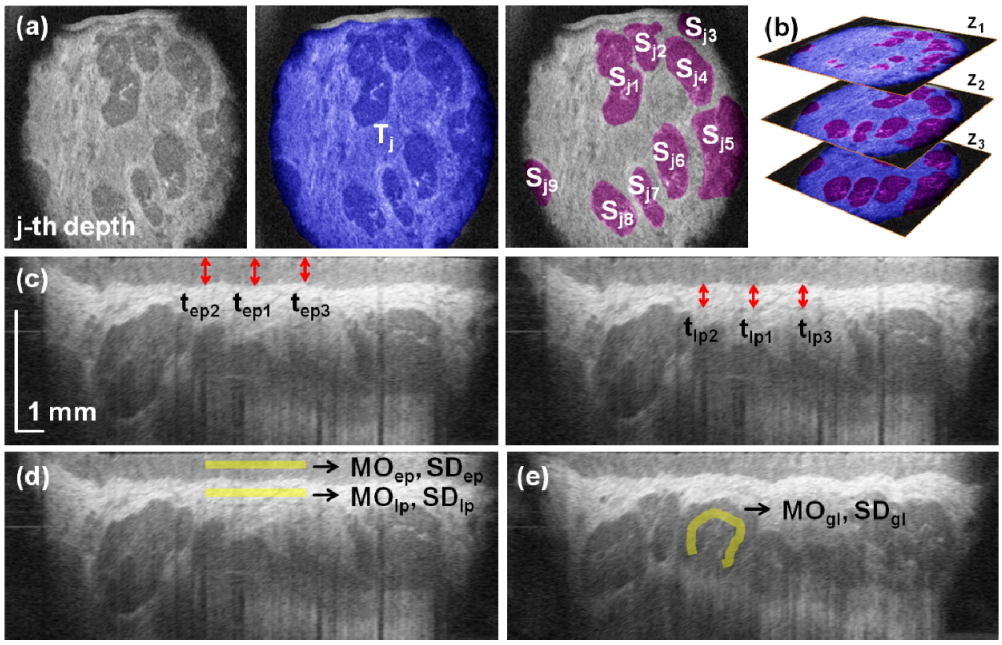

Fig. 2. Quantitative assessment of the mucosa of the lower lip and LMSGs. (a) Observable mucosal tissue (blue) and individual glands (violet) were segmented to determine the corresponding areas. (b) The analyses were performed at three depths to provide with volumetric analysis. (c) Measurement of the average thickness of the epithelium (left) and the hyperreflective part of the lamina propria (right). (d) Estimation of the reflectivity and heterogeneity of the epithelium and the lamina propria. (e) Estimation of the reflectivity and heterogeneity of the glandular tissue.

Stacks of C-scans and B-scans (both 8-bit jpg-files) were manually analyzed using Fiji image processing package [48]. A set of morphometric parameters was chosen to reflect LMSGs' size, surface density, and optical properties of their glandular tissue. Thickness and optical properties of the epithelium and the adjacent lamina propria were investigated.

Following preliminary observations of LMSGs in C-scans three tissue depths (z_1 = 500 µm, z_2 = 650 µm, and z_3 = 800 µm) were chosen for further analyses on the basis of the presence of LMSGs and image quality. Manual segmentation of glands in each selected projection image allowed for determination of the following descriptors: area of glands S_j, area of observable mucosal tissue T_j and the number of the visualized glands n_j (Fig. 2(a)). They were later used to define the following parameters:

#199754 - $15.00 USD Received 23 Oct 2013; revised 26 Nov 2013; accepted 26 Nov 2013; published 16 Dec 2013

- **LMSG surface filling factors** defined as the ratio of the area occupied by LMSGs in particular C-scans (at z_1, z_2 or z_3) to the corresponding observable area of the mucosa:

$$FF_j = S_j / T_j, \tag{1}$$

where: $S_j = \sum_{i=1}^{n_j} S_{ji}$ is the total LMSG area in *j*-th depth, S_{ji} stands for the area of the *i*-th gland at *j*-th depth (Fig. 2(a)), n_j stands for the number of identified glands at *j*-th C-scan and the index *j*(= 1, 2, 3) corresponds to the depths z_1, z_2 and z_3, respectively,

- **depth-integrated LMSG surface filling factor** defined as the ratio of the sum of LMSGs' surfaces in C-scans at z_1, z_2 and z_3 to the sum of tissue surfaces visible at those depths (Fig. 2(b)):

$$IFF = \sum_{j=1}^{3} S_j \Big/ \sum_{j=1}^{3} T_j, \tag{2}$$

- **LMSGs' surface densities** in C-scans at z_1, z_2 and z_3, defined as the number of glands distributed over corresponding mucosal tissue area:

$$\rho_j = n_j / T_j, \tag{3}$$

- **depth-integrated LMSGs' surface density** defined as the sum of LMSGs' numbers in C-scans at z_1, z_2 and z_3, divided by the sum of the mucosal tissue areas visible at those depths:

$$\rho = \sum_{j=1}^{3} n_j \Big/ \sum_{j=1}^{3} T_j, \tag{4}$$

- **average single LMSG area at z_j** and **average single LMSG area in tissue sample** defined by the following equations:

$$\overline{A}_j = S_j / n_j \quad \text{and} \quad \overline{A} = \sum_{j=1}^{3} S_j \Big/ \sum_{j=1}^{3} n_j. \tag{5}$$

The structure revealed in cross-sectional images (B-scans) was also investigated. Central B-scan was extracted from the volumetric data set and here the measured parameters included:

- **average thickness of the epithelium** based on the measurements at the central A-scan (t_{ep1}) and at its both sides (t_{ep2} and t_{ep3}), each 1.7 mm away from the center (Fig. 2(c)):

$$t_{ep} = \frac{1}{3} \sum_{i=1}^{3} t_{epi}, \tag{6}$$

- **average thickness of the hyperintensive part of the lamina propria**, which was directly underlying the epithelium, based on the measurements at the central A-scan (t_{lp1}) and at its both sides (t_{lp2} and t_{lp3}), each 1.7 mm away from the center (Fig. 2(c)):

$$t_{lp} = \frac{1}{3} \sum_{i=1}^{3} t_{lpi}, \tag{7}$$

#199754 - $15.00 USD Received 23 Oct 2013; revised 26 Nov 2013; accepted 26 Nov 2013; published 16 Dec 2013

- **epithelium reflectivity** described by the mode MO_{ep} of the signal of the epithelium, as measured in a region of interest (rectangle 34 μm wide and 3.4 mm long) drawn in the middle of the epithelial layer (Fig. 2(d)),
- **epithelium heterogeneity** described by the standard deviation SD_{ep} of the signal in this area (Fig. 2(d)),
- **lamina propria reflectivity** described by the mode MO_{lp} of the signal from the hyperintensive part of the lamina propria, as measured in a region of interest (rectangle 34 μm wide and 3.4 mm long) drawn in the middle of the lamina propria (Fig. 2(d)),
- **lamina propria heterogeneity** described by the standard deviation SD_{lp} of the signal in this area (Fig. 2(d)).

Three selected B-scans were also chosen to assess **glandular tissue reflectivity** defined by the mode MO_{gl} of the signal of the glandular tissue, as measured in a 34 μm wide channel of varying length drawn in LMSGs visible in selected B-scans (Fig. 2(e)). Simultaneously, **glandular tissue heterogeneity** was determined by the measurement of the standard deviation SD_{gl} of the signal in these areas.

Extraction of the parameters from a single data set took only few minutes since it required segmentation of the mucosal tissue and individual glands in three projection planes as well as analysis of few cross-sections for thickness, reflectivity and heterogeneity of the tissues. The time needed for extraction of the parameters used in this study is not significantly longer than analysis of a histopathological sample or a morphometric analysis of an ultrasound image. The data were read automatically with a pen and immediately transferred to the data sheet.

Statistical analyses were carried out using STATISTICA data analysis software system (v. 10; StatSoft Inc., Tulsa, OK, USA). The Shapiro-Wilk test was employed to assess the normality of distribution of continuous parameters in groups and subgroups. The Mann-Whitney U test was applied to compare distributions of parameters between patients with Sjögren's syndrome and the control group as well as between Sjögren's syndrome patients with and without prespecified clinical characteristics. The significance level was set at $p < 0.05$. The data are presented as median and interquartile range unless stated otherwise. Reproducibility was assessed using one-way ANOVA with a random-effects model. Variance analysis enabled computation of intraclass correlation coefficient (ICC) and intersession standard deviation (SD) for each measured parameter.

3. Results

3.1 In vivo OCT imaging of the labial minor salivary glands

High-speed SS-OCT enables volumetric imaging of the oral mucosa. Figure 3 demonstrates wide-field OCT data set covering 17.3 × 17.3 mm^2 area of the inner surface of the lower lips. Raster scanning of the tissue allows for acquisition of multiple cross-sections that are later used to reconstruct the structures in three dimensions (Fig. 3(a)). Cross-sectional OCT images in Fig. 3(b) reveal characteristic features of the oral mucosa. The tissue surface was segmented for flattening procedure. Different scattering properties allow for delineation of the layers such as the epithelium and the lamina propria. Hyporeflective structures are the LMSGs.

Enhanced light penetration at 1.3 μm and high sensitivity of the instrument facilitates acquisition of signals from the tissues below the glands. Access to volumetric data provides comprehensive information on the imaged structures and makes generation of any section possible. Although en-face (depth-integrated) image has limited value (Fig. 3(c)), subsurface features can be extracted from projection (C-scan) images. Connective tissue demonstrates higher reflectivity than the glands (Fig. 3(d)).

#199754 - $15.00 USD Received 23 Oct 2013; revised 26 Nov 2013; accepted 26 Nov 2013; published 16 Dec 2013

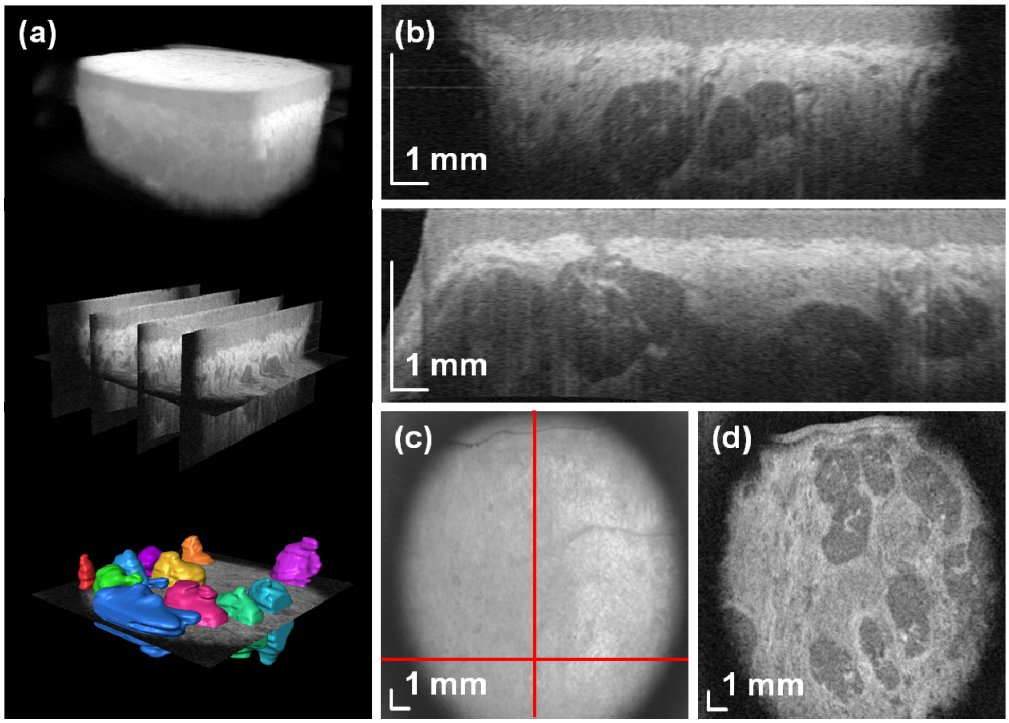

Fig. 3. *In vivo* wide-field SS-OCT imaging of the labial minor salivary glands. (a) Rendering of the volumetric data set along with segmented glands (Media 1). (b) Two cross-sectional images (B-scans) of the mucosal tissue. (c) En-face image. (d) C-scan image at depth z = 657 μm showing rich glandular tissue. A flythrough demonstrating structures at different depths (Media 2).

Performance of the developed SS-OCT instrument can be demonstrated when denser lateral scanning is applied. Therefore, we reduced scanned area by a factor of 9 compared to the previous case (5.8 × 5.8 mm^2). We aligned the field of view so that the entire group of salivary glands was positioned at the center of the scanned area. An example showed in Fig. 4 shows that the gland is composed of three lobules. 3-D rendering allows for generation of different sections (Fig. 4(a)). Organization of the human oral mucosa enables identification of small features like an excretory (interlobular) duct that was associated with the salivary unit of interest (Fig. 4(b)). Good image quality enables segmentation of the glands for three-dimensional visualization (Fig. 4(c)). Due to better sampling, it is possible to see characteristic pattern of the epithelial cells in the projection image close to the mucosa surface (Fig. 4(d)). In addition, deeper C-scans present details of the glands along with their vascularization. It is worth noting that glandular tissue is not homogeneous. The connective tissue can be seen filling the space between the lobules.

#199754 - $15.00 USD Received 23 Oct 2013; revised 26 Nov 2013; accepted 26 Nov 2013; published 16 Dec 2013

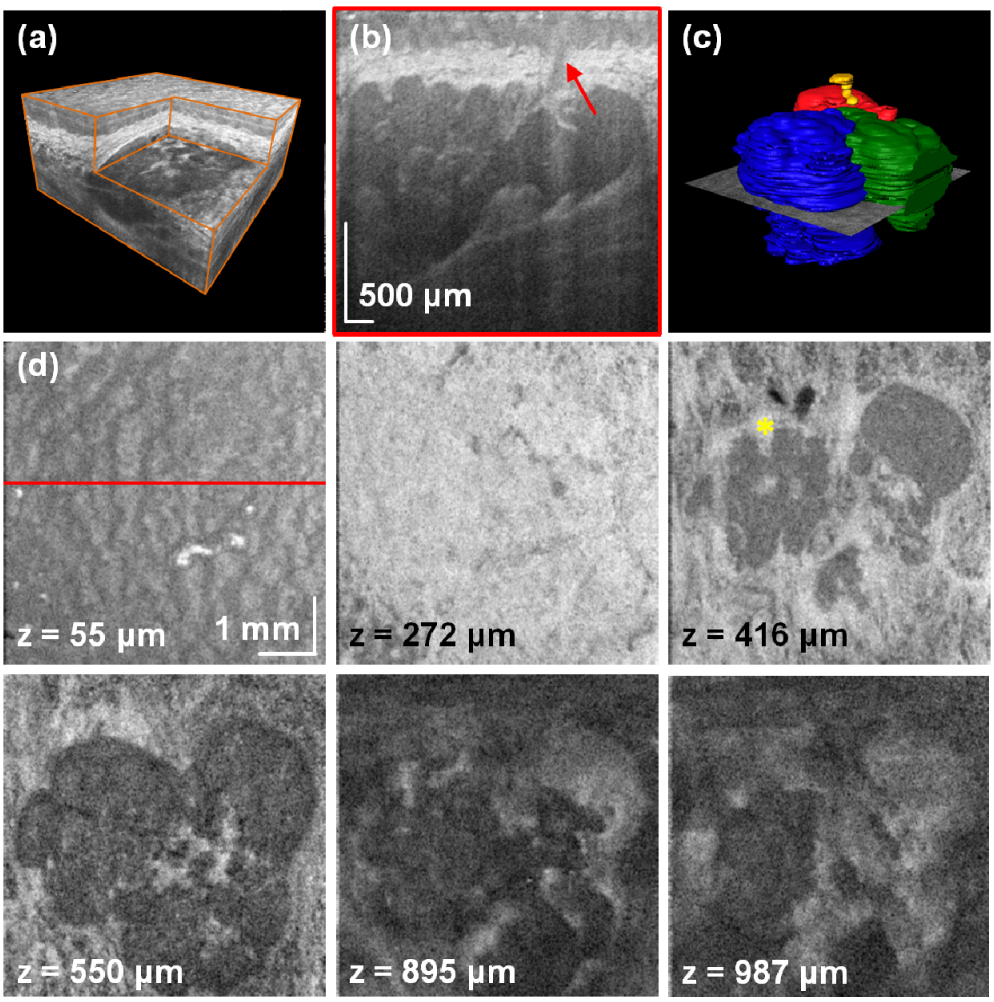

Fig. 4. High-definition imaging of the LMSGs. (a) Rendering of the volumetric data set with the corner cut. (b) Cross-sectional image of the mucosal tissue. The arrow indicates the excretory salivary duct. (c) Segmentation of the glandular units and the salivary duct (Media 3). (d) C-scans at different depths showing anatomical features of the mucosa and details of the glandular tissue. Asterisk indicates blood vessels in oral mucosa. A flythrough demonstrating structures at different depths (Media 4).

3.2 Assessment of the measurement approach

The control group and patients were measured using wide-field scanning protocol. The oral mucosa of each person was measured in three scanning sessions. The extracted C-scans and B-scans were used for quantitative analysis. The results of variance analysis (ANOVA) of repeated measurements are presented in Table 2. All parameters except glandular tissue reflectivity MO_{gl} show very good intersession reproducibility with statistical significance.

#199754 - $15.00 USD Received 23 Oct 2013; revised 26 Nov 2013; accepted 26 Nov 2013; published 16 Dec 2013

Table 2. Intersession reproducibility of the measurement of mucosal tissue morphometric parameters

Parameter	Intersession SD	ICC
Depth-integrated LMSG surface filling factor (IFF)	0.026	0.9520
LMSG surface filling factor at z_1 (FF_1)	0.036	0.9164
LMSG surface filling factor at z_2 (FF_2)	0.037	0.9209
LMSG surface filling factor at z_3 (FF_3)	0.031	0.9335
Depth-integrated LMSGs' surface density (ρ), cm^{-2}	0.46	0.9541
LMSGs' surface density at z_1 (ρ_1), cm^{-2}	0.93	0.8906
LMSGs' surface density at z_2 (ρ_2), cm^{-2}	0.67	0.9136
LMSGs' surface density at z_3 (ρ_3), cm^{-2}	0.83	0.7961
Average single LMSG area A in tissue sample, mm^2	0.59	0.8218
Average single LMSG area A_1 at z_1, mm^2	0.62	0.8213
Average single LMSG area A_2 at z_2, mm^2	0.94	0.6928
Average single LMSG area A_3 at z_3, mm^2	0.98	0.6205
Thickness of the epithelium t_{ep}, µm	19.2	0.8900
Thickness of the hyperintensive part of the lamina propria t_{lp}, µm	15.9	0.7936
Epithelium reflectivity MO_{ep}	3.8	0.9144
Epithelium heterogeneity SD_{ep}	0.84	0.6472
Lamina propria reflectivity MO_{lp}	6.7	0.8306
Lamina propria heterogeneity SD_{lp}	1.3	0.4874 †
Glandular tissue reflectivity MO_{gl}	12.1	0.6650
Glandular tissue heterogeneity SD_{gl}	1.6	0.8618

*Tissue depths: z_1 = 500 µm, z_2 = 650 µm, z_3 = 800 µm. ICC – intraclass correlation coefficient, LMSG – labial minor salivary gland, MO – mode, SD – standard deviation.
†No statistical difference found.

3.3 Comparison of the morphometry of the lower lip mucosa between healthy subjects and Sjögren's syndrome patients

The average areas of tissue visible in selected C-scans measured at the depths z_1, z_2 and z_3 were 1.93 cm^2, 1.86 cm^2, and 1.82 cm^2, respectively. The median values of the morphometric parameters measured in patients with Sjögren's syndrome and in control group are summarized in Table 3. No statistically significant differences between Sjögren's syndrome patients and the control group were observed. We also analyzed subgroups of Sjögren's syndrome patients based on the questionnaire items. We found differences in distributions of the morphometric parameters in patients suffering from xerostomia-related dental disease, Raynaud's phenomenon, and those who were treated with chloroquine.

In patients with Sjögren's syndrome with xerostomia-related dental disease (5 patients) distributions of 5 parameters differed from those found in the rest of patients with Sjögren's syndrome (6 patients). The median values, interquartile ranges and p values are presented in Table 4. Information on the standard deviation of the signal of the epithelium and the glandular tissue in OCT images in both subgroups were also added to Table 4. The median value of the standard deviation of the signal of the epithelium in patients with Sjögren's syndrome with xerostomia-related dental disease was greater than in the control group (12 (12-13) vs. 10 (9-12), p = 0.04).

In patients with Sjögren's syndrome who experienced Raynaud's phenomenon (5 patients) the median depth-integrated LMSG surface filling factor (IFF) was higher than in the rest of patients with Sjögren's syndrome (0.14 (interquartile range 0.10-0.15) vs. 0.05 (0.04-0.06), p = 0.03). Moreover, the median LMSG surface filling factor at z_2 was higher in patients with history of Raynaud's phenomenon than in the rest of patients with Sjögren's syndrome (0.15 (0.15-0.16) vs. 0.06 (0.02-0.09), p = 0.03). However, the differences in distribution of the

#199754 - $15.00 USD Received 23 Oct 2013; revised 26 Nov 2013; accepted 26 Nov 2013; published 16 Dec 2013

average single LMSG area in tissue sample were statistically non-significant (3.39 mm^2 (3.12-3.86) vs. 2.50 mm^2 (2.09-2.88); p = 0.05).

Table 3. Morphometric parameters of the inner surface of the lower lip measured in Sjögren's syndrome patients and in the control group

Parameter	Sjögren's syndrome patients	Control group
Depth-integrated LMSG surface filling factor (IFF)	0.06 (0.04-0.14)	0.09 (0.04-0.24)
LMSG surface filling factor at z_1 (FF_1)	0.03 (0.01-0.05)	0.06 (0.00-0.19)
LMSG surface filling factor at z_2 (FF_2)	0.09 (0.06-0.15)	0.10 (0.03-0.24)
LMSG surface filling factor at z_3 (FF_3)	0.12 (0.08-0.16)	0.13 (0.08-0.27)
Depth-integrated LMSGs' surface density (ρ), cm^{-2}	2.89 (2.16-3.13)	2.86 (1.69-5.54)
LMSGs' surface density at z_1 (ρ_1), cm^{-2}	2.40 (1.09-3.22)	3.39 (0.00-6.85)
LMSGs' surface density at z_2 (ρ_2), cm^{-2}	3.16 (3.00-4.06)	3.05 (0.58-6.30)
LMSGs' surface density at z_3 (ρ_3), cm^{-2}	2.79 (2.20-4.23)	3.86 (2.58-5.18)
Average single LMSG area A in tissue sample, mm^2	2.88 (2.15-3.39)	3.29 (2.33-4.00)
Average single LMSG area A_1 at z_1, mm^2	1.57 (1.15-1.98)	1.83 (1.26-3.75)
Average single LMSG area A_2 at z_2, mm^2	2.01 (1.59-3.89)	3.21 (1.28-4.46)
Average single LMSG area A_3 at z_3, mm^2	4.44 (3.01-6.07)	4.36 (3.14-4.85)
Thickness of the epithelium t_{ep}, µm	245 (209-289)	210 (190-302)
Thickness of the hyperintensive part of the lamina propria t_{lp}, µm	204 (147-242)	182 (166-198)
Epithelium reflectivity MO_{ep}	159 (148-166)	161 (151-173)
Epithelium heterogeneity SD_{ep}	11 (10-12)	10 (9-12)
Lamina propria reflectivity MO_{lp}	202 (185-214)	201 (198-223)
Lamina propria heterogeneity SD_{lp}	11 (10-13)	12 (11-14)
Glandular tissue reflectivity MO_{gl}	70 (61-89)	67 (58-79)
Glandular tissue heterogeneity SD_{gl}	13 (12-16)	16 (12-18)

*The data are presented as median (interquartile range). Tissue depths: z_1 = 500 µm, z_2 = 650 µm, z_3 = 800 µm. LMSG – labial minor salivary gland, MO – mode, SD – standard deviation.

In patients with Sjögren's syndrome treated with chloroquine (4 patients) the distribution of LMSGs' surface density at z_3 differed from the one found in the rest of patients with Sjögren's syndrome (7 patients). The median values were higher in chloroquine-receiving subjects (3.70 cm^{-2} (3.16-5.58) vs. 2.60 cm^{-2} (1.50-2.79); p = 0.04). The distribution of mode of the signal from the epithelium also differed between the two groups, with lower median of mode of the signal observed in patients taking chloroquine (147 (146-155) vs. 163 (157-167), p = 0.04).

Table 4. Comparison of the morphometric parameters in patients with Sjögren's syndrome with and without xerostomia-related dental disease

Parameter	Xerostomia-related dental disease	No xerostomia-related dental disease	p value
Depth-integrated LMSG surface filling factor (IFF)	0.14 (0.09-0.15)	0.05 (0.04-0.06)	0.03
LMSG surface filling factor at z_1 (FF_1)	0.05 (0.04-0.10)	0.01 (0.00-0.03)	0.02
LMSGs' surface density at z_2 (ρ_2), cm^{-2}	4.06 (3.19-4.57)	3.04 (2.66-3.09)	0.02
Average single LMSG area A in tissue sample, mm^2	3.13 (3.02-3.63)	2.26 (1.75-2.89)	0.01
Epithelium heterogeneity SD_{ep}	12 (12-13)	10 (9-11)	0.03
Glandular tissue heterogeneity SD_{gl}	16 (15-16)	13 (12-13)	0.05

*The data are presented as median (interquartile range). Tissue depths: z_1 = 500 µm, z_2 = 650 µm, z_3 = 800 µm. LMSG – labial minor salivary gland, SD – standard deviation.

All participants assessed also the levels of anxiety before the measurements and comfort during data acquisition. The average level of anxiety before OCT scanning was 4.6 (5 = not anxious at all) and the average rating of comfort during OCT scanning was 4.8 (5 = very good).

4. Discussion

The prototype SS-OCT system presented in this report was applied in the assessment of the oral mucosa. The system operates at 1.3 µm, which allows for deeper penetration of light into

#199754 - $15.00 USD Received 23 Oct 2013; revised 26 Nov 2013; accepted 26 Nov 2013; published 16 Dec 2013

opaque tissue compared to other wavelengths used in OCT technology. Moreover, a very good instrument performance in terms of signal roll-off with depths enables application of the specific scanning approach, in which tissue imaging through the glass plate is performed. Deep light penetration and optimized signal roll-off with depth are advantageous for the presented application since visualization of entire gland structure can be done. Since the system has ~3.4 mm depth range and low signal drop, the glass plate can be tilted and no significant image quality degradation for different transverse depth scans is observed. Furthermore, application of the glass plate in the sample arm makes the quantitative analysis more valid since the focus position is well reproduced for each scanned person.

High-speed SS-OCT enables also in vivo imaging and acquisition of three-dimensional data sets. Access to the volumetric data enables extraction of virtually any cross-sectional image. The employed method provided high quality volumetric images of the mucosa of the lower lip that were clear until the depth of 800 μm. Although the obtained resolution was lower than in modern microscopy, it was sufficient to visualize the details of the oral mucosa. Structures typical of the analyzed tissue, such as non-keratinized stratified squamous epithelium, LMSGs, LMSGs' excretory ducts, connective tissue of the lamina propria, blood vessels and parts of the muscular layer were readily visible. In conjunction with the large scan area (~230 mm^2) access to volumetric data leads to the comprehensive analysis of the morphology of the labial minor salivary glands. To the best of our knowledge, this is the first report showing quantitative parameters of the glandular tissue of the lower lip and comparison of morphological features between healthy subjects and patients with Sjögren's syndrome. Measured thickness of the epithelium and LMSGs' surface density correspond to results obtained earlier [16, 49]. The chosen parameters had good intraclass correlation coefficients.

Possible source of error (variation) may come mainly from pressure / force levels applied when the patients touched the glass plate. The pressure exerted on the glass plate by each study participant was not controlled, thus it could have been slightly different, which may have affected the tissue morphometry. To make sure we do not introduce additional variation of the parameters due to different force levels applied to the glass, we did additional experiments before the study. The same person pressed his / her lip against the glass with different force. However, we did not observe any differences in the measured parameters within a reasonable range of pressure (force) levels.

Another limitation of the study was relatively small sample size. The fact that the differences were statistically significant notwithstanding the small subgroup sizes suggests that the observed clinical phenomenon could be very strongly pronounced, e.g. in five out of six Sjögren's syndrome patients without xerostomia-related dental diseases the IFF was lower than in four out of five patients with xerostomia-related dental disease. The Mann-Whitney U test that we employed was highly robust, giving the p value of 0.03. In this particular case testing for normality using the Kolmogorov–Smirnov test and the Lilliefors test suggested that value distributions in subgroups were normal and thus Student's t-test could be employed. Although we obtained promising results, they should be interpreted carefully until studies with larger sample sizes are performed.

No statistically significant disparities in the measured parameters between patients with Sjögren's syndrome and the control group were observed. It is possible that at this resolution there are no diagnostically useful differences in mucosal morphology between patients with Sjögren's syndrome and subjects without Sjögren's syndrome. As there are studies suggesting that labial gland function and morphology may change in Sjögren's syndrome under the influence of pharmacotherapies, it must be emphasized that treatment was not withdrawn in patients with Sjögren's syndrome because of ethical concerns [50, 51]. On the other hand, progression of LMSGs' fibrosis during long-term steroid treatment of Sjögren's syndrome has been documented [52]. Moreover, all the patients in the studied group experienced xerostomia regardless of employed therapies. In the future, the paucity of data on the

#199754 - $15.00 USD Received 23 Oct 2013; revised 26 Nov 2013; accepted 26 Nov 2013; published 16 Dec 2013

influence of pharmacotherapies on LMSGs' morphology could be addressed by the use of OCT.

The analyses of the Sjögren's syndrome patient subgroups identified differences that could be partially explained by the LMSG pathophysiology. In patients with Sjögren's syndrome and xerostomia-related dental disease IFF was greater, reflecting a larger total LMSG volume. This resulted from both larger LMSGs' surface density and greater average single LMSG area, indicating a larger single LMSG volume. The epithelium in this subgroup was also more heterogenous. Xerostomia-related dental disease is found in patients with highly active Sjögren's syndrome in whom LMSG histopathological changes are most severe, leading to a significant decrease in salivary flow [53–55]. Observed changes in LMSG may be due to increased inflammation, which is linked to major salivary glands enlargement, a clinical hallmark of active Sjögren's syndrome [1]. The greater epithelial heterogeneity could be a consequence of increased mucosal stress due to the lack of saliva.

Greater IFF in patients with Raynaud's phenomenon could also point to a more active inflammation. However, although patients that experience Raynaud's phenomenon have distinct immunological characteristics of Sjögren's syndrome [56], so far they were shown to be linked only to extraglandular disease manifestations.

In patients with Sjögren's syndrome taking chloroquine the lower epithelium reflectivity could result from a drug-induced pigmentation [57]. Chloroquine was shown to increase salivary flow in Sjögren's syndrome by improving the function of glandular cholinesterase [58]. However, this mechanism does not explain the increased LMSGs' surface density at z_3.

7. Summary and conclusions

To summarize, this manuscript reported SS-OCT for *in vivo* oral mucosa imaging at 1310 nm. Wide-field volumetric imaging of the inner surface of the lower lip was demonstrated in patients with Sjögren's syndrome and in a control group. Visualization and quantitative assessment of the labial minor salivary glands were performed for the first time. The method of extracting morphometric parameters of the labial glands from OCT data was developed and repeatability of the proposed parameters was confirmed. No statistically significant differences between both studied groups were found. However, statistically significant differences were observed in Sjögren's syndrome patients when selection criteria, such as the presence of: xerostomia-related dental disease, Raynaud's phenomenon or treatment with chloroquine, were taken into account. Application of OCT in LMSGs imaging opens new gates for the assessment and understanding of the changes of the mucosa of the lower lip in a range of diseases affecting the oral cavity. Both high performance and noninvasiveness of SS-OCT promise to enable fast diagnosis of the morphologic state of LMSGs.

Acknowledgments

The study is supported by the National Science Center within the MAESTRO Programme (#DEC-2011/02/A/ST2/00302) and a grant from Poznań University of Medical Sciences. IG acknowledges also the scholarship of the Polish Ministry of Science and Higher Education. The authors would like to express their gratitude to Anna Rychlewska-Hańczewska, MD, for her help with patient recruitment.

#199754 - $15.00 USD Received 23 Oct 2013; revised 26 Nov 2013; accepted 26 Nov 2013; published 16 Dec 2013